4f–5d spectroscopy of Ce^{3+} in $CaBPO_5$, $LiCaPO_4$ and Li_2CaSiO_4

2003 J. Phys.: Condens. Matter 15 511

(http://iopscience.iop.org/0953-8984/15/3/315)

INSTITUTE OF PHYSICS PUBLISHING JOURNAL OF PHYSICS: CONDENSED MATTER

J. Phys.: Condens. Matter **15** (2003) 511–520 PII: S0953-8984(03)55449-2

4f–5d spectroscopy of Ce^{3+} in $CaBPO_5$, $LiCaPO_4$ and Li_2CaSiO_4

P Dorenbos[1], L Pierron[2], L Dinca[1], C W E van Eijk[1], A Kahn-Harari[2] and B Viana[2]

[1] Interfaculty Reactor Institute, Delft University of Technology, Mekelweg 15, 2629 JB Delft, The Netherlands
[2] Ecole Nationale Supérieure de Chimie de Paris (ENSCP), Laboratoire de Chimie Appliquée de l'Etat Solide, UMR-CNRS 7574, 11 rue Pierre et Marie Curie, 75231 Paris cedex 05, France

E-mail: dorenbos@iri.tudelft.nl

Received 1 November 2002
Published 13 January 2003
Online at stacks.iop.org/JPhysCM/15/511

Abstract

The properties of Ce^{3+} in $CaBPO_5$, $LiCaPO_4$ and Li_2CaSiO_4 have been studied in the 100–400 nm wavelength region with time resolved spectroscopy at temperatures between 10 and 300 K. Emphasis is on the relationship between the energies of the five 5d levels of Ce^{3+} and the crystalline environment. Good agreement between predicted and observed average energy of the 5d configuration is demonstrated. In addition values for the bandgap of the host materials, Stokes shifts and luminescence decay time data are presented.

1. Introduction

For gamma ray detection purposes, we recently developed high light output, heavy and fast scintillators based on Ce^{3+} in crystalline compounds [1–3]. High densities ($\rho = 5$–$8\ g\ cm^{-3}$) of the host crystals are a requirement for an efficient detection of gamma rays. For the detection of thermal neutrons different requirements are imposed. The host crystal should contain ^6Li or ^{10}B because these isotopes provide large capture cross-section for thermal neutrons. Subsequent decay of the unstable nucleus after neutron capture leads to the creation of a scintillation pulse. In addition the compound should be insensitive to gamma rays. The low density of $CaBPO_5$, $LiCaPO_4$ and Li_2CaSiO_4 combined with the presence of one of the required isotopes make them interesting for such application.

They are also of interest from a more fundamental point of view. In each compound there is only one type of Ca site. Ce^{3+} has about the same size as Ca^{2+} and large lattice relaxation around Ce^{3+} is not expected. The effects of coordination and anion properties on the 5d levels of Ce^{3+} can then be nicely studied. Not much is known on the spectroscopic properties of lanthanide 5d levels in these compounds. Some studies on Eu^{2+} and Sm^{2+} doped $CaBPO_5$

have been reported [4–7]; Eu^{2+} doped $LiCaPO_4$ has also been studied [8], but information on Li_2CaSiO_4 was not found.

This work is organized as follows. First, as an introduction, some aspects of Ce^{3+} spectroscopy will be reviewed. Next, results from vacuum ultraviolet and ultraviolet spectroscopy will be presented. It provides the information on the 5d levels from which parameters like redshift, centroid shift, crystal field splitting and Stokes shift are obtained. Finally these properties will be compared with that in other compounds and predictions from phenomenological models.

2. General aspects of Ce^{3+} spectroscopy

The spin–orbit split $^2D_{3/2}$ and $^2D_{5/2}$ states of the 5d configuration of free Ce^{3+} are located 49 700 and 52 100 cm^{-1} above the $4f^1\ ^2F_{5/2}$ ground state of Ce^{3+} [9]. When Ce^{3+} is introduced in a compound the average energy of the 5d configuration is lowered and the $^2D_{3/2}$ and $^2D_{5/2}$ states are further split by the crystal field. Depending on the site symmetry at most five distinct 5d states may form. Due to the strong electron–phonon coupling between 5d electron and lattice vibrations, vibronic side bands develop next to the zero-phonon lines. The zero-phonon lines are usually absent or very weak and only the broad vibronic side bands are observed in fd excitation and emission spectra. In this work we will only deal with the side bands and we will refer to them as the 5d bands.

The energy difference between the maxima of the highest and lowest 5d band in spectra is defined as the total crystal field splitting ϵ_{cfs}. The energy shift of the average of the 5d configuration is defined as the centroid shift ϵ_c [10]. The combination of ϵ_c and ϵ_{cfs} leads to the redshift D defined as

$$D = 49\,340 - \frac{10^7}{\lambda_1}\ \mathrm{cm}^{-1} \tag{1}$$

where λ_1 is the wavelength (nm) of the first 5d absorption band in Ce^{3+}. The energy difference between the first fd transition and the df emission to the $^2F_{5/2}$ ground state is defined as the Stokes shift ΔS. Values for the redshift and Stokes shift of Ce^{3+} are available in many different compounds [11].

It was found that ϵ_{cfs} can be analysed in terms of the type and size of anion coordination polyhedron around Ce^{3+} [12, 13]. Figure 1 compiles data on ϵ_{cfs} of Ce^{3+} in a variety of compounds. When the shape of the coordination polyhedron remains the same, ϵ_{cfs} behaves as

$$\epsilon_{cfs} = \beta R_{av}^{-2} \tag{2}$$

where β is a constant that depends on the shape of the polyhedron. R_{av} is defined as

$$R_{av} = 1/N \sum_{i=1}^{N} (R_i - 0.6\Delta R), \tag{3}$$

and represents the average distance to the coordinating ligands in the relaxed lattice structure around Ce^{3+}. R_i (pm) are the bond lengths to the N coordinating anions in the unrelaxed lattice. ΔR is the difference of ionic radius between Ce^{3+} and the cation it substitutes for. In the case of Ca, $\Delta R = -2$ pm. Note that the properties of the anions, i.e., the type of anion or whether the anions are strongly bonded in anionic complexes, do not appear in equation (2). The dashed curves running through the data in figure 1 are described by equation (2).

The magnitude of ϵ_c is determined by the polarizability of anion ligands, the covalency between anions and Ce^{3+} and the nephelauxetic effect. All three contributions can be expressed

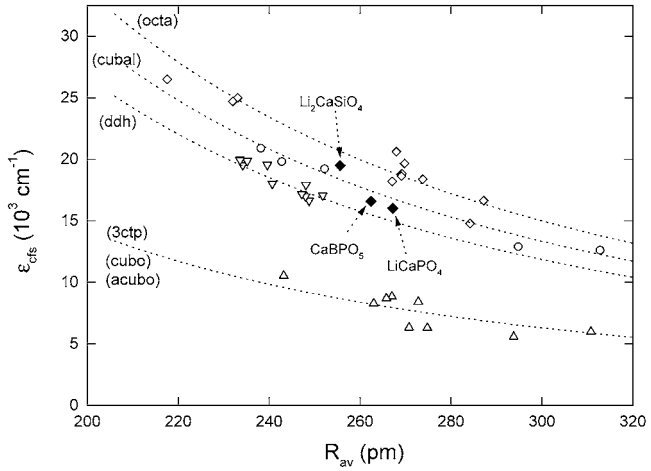

Figure 1. The crystal field splitting of Ce^{3+} 5d levels in compounds with ◊ octahedral, ▽ dodecahedral, O cubal and △ tricapped trigonal prism, cuboctahedral and anti-cuboctahedral coordination.

by the spectroscopic polarizability α_{sp} (10^{-30} m^3) which can be calculated without any fitting parameter from the observed centroid shift using [10]

$$\alpha_{sp} = \frac{6.9 \times 10^{-18} \epsilon_c}{\sum_{i=1}^{N} (R_i - 0.6\Delta R)^{-6}}. \tag{4}$$

There exists a phenomenological linear relationship between α_{sp} and the weighted average χ_{av} of the electronegativity of the cations in oxide compounds [14]

$$\alpha_{sp} = 0.33 + \frac{4.8}{\chi_{av}^2}. \tag{5}$$

Figure 2 shows this linear relationship displayed by about 50 different Ce^{3+} doped compounds. For $CaBPO_5$, $LiCaPO_4$ and Li_2CaSiO_4 with $\chi_{av} = 1.91$, 1.74 and 1.45, equation (5) predicts 1.65, 1.92 and 2.63 $\times$ 10^{-30} m^3 for α_{sp}, respectively. With R_i determined from the crystal structure, centroid shifts of 8240, 8940 and 11 600 cm^{-1} are then anticipated for these three compounds, respectively.

3. Experimental techniques and crystal properties

Polycrystalline powder of Li_2CaSiO_4 with calculated density $\rho = 2.9$ g cm^{-3} was prepared by solid state reaction of stoichiometric mixtures of Li_2CO_3, $CaCO_3$, SiO_2 and CeO_2 under argon atmosphere at 900 °C for 9 h in a pyrox tubular furnace. A pure sample and a sample with 0.5% Ce^{3+} were prepared. X-ray diffraction showed that the materials are of single phase. Since Ce^{3+} are located on the divalent Ca sites some sort of charge compensating defect will be built in the lattice. We did not add a charge compensating codopant to the compound, therefore some intrinsic compensation mechanisms will take place. $CaBPO_5$ with calculated density of $\rho = 3.2$ g cm^{-3} was prepared from a stoichiometric mixture of $CaCO_3$, H_3BO_3, $NH_4H_2PO_4$, CeF_3 and Na_2CO_3, treated under argon atmosphere at 900 °C for 6 h. After grinding the product, it was followed by a treatment at 920 °C for 15 h. Na^+ on a Ca^{2+} site acts as a charge compensating defect.

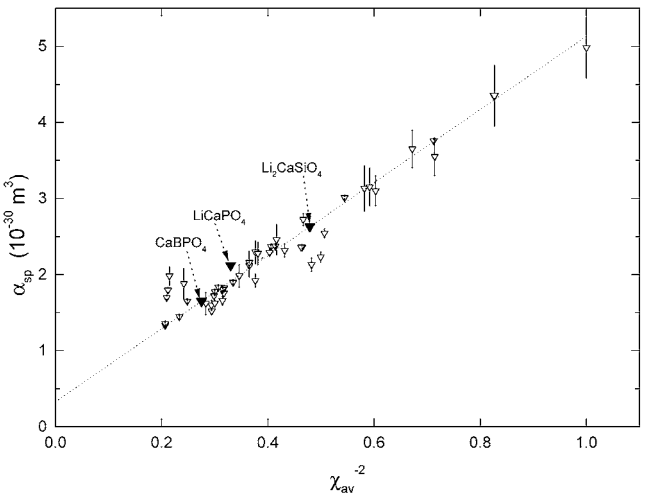

Figure 2. Spectroscopic polarizability in oxide compounds.

Pure $LiCaPO_4$ with calculated density $\rho = 2.9$ g cm^{-3} was prepared by mixing stoichiometric quantities of Li_2CO_3, $CaCO_3$ and $NH_4H_2PO_4$ and heating them under argon atmosphere. Several heating steps were required to remove intermediary products until finally the right phase was formed. By adding CeF_3 in between two of these steps, the Ce doped material was prepared. The undoped material appears to be of satisfactory pure phase, but the doped material contains some $Ca_2P_2O_7$ as an impurity phase.

All samples are either undoped or prepared with a Ce^{3+} concentration of 0.5 mol% weighted in the starting materials. The final Ce^{3+} concentration was not analysed and is probably lower. Spectroscopic techniques did reveal impurity traces of Gd^{3+} and Ce^{3+} in the undoped materials. These impurities come from the raw materials.

Excitation and emission spectroscopy were performed by UV/VIS and VUV spectroscopic techniques. Time resolved excitation spectra at 12 K and room temperature were performed at the Superlumi VUV station of the DESY synchrotron facility in Hamburg, Germany. The synchrotron operated in multi-bunch mode with bunches separated by 200 ns. Three types of excitation spectra were recorded. The 'fast' excitation spectra were obtained by monitoring the light emitted at wavelength λ in a 12 ns time window starting 1.5 ns after the excitation pulse. The 'slow' spectra were obtained using an 85 ns wide time window starting after 74 ns delay. The 'integral' spectra were obtained using all light emitted at wavelength λ. The excitation spectra were corrected for the spectral shape of the excitation source by means of a Na salicylate reference measurement.

4. Results

The emission spectra of the three Ce^{3+} doped compounds under excitation to one of the levels of the 5d configuration are shown in figure 3. For each compound two emission bands separated by about 2000 cm^{-1} are observed. They are due to transitions to the spin–orbit split $^2F_{5/2}$ and $^2F_{7/2}$ levels of the $4f^1$ configuration of Ce^{3+}. The doublet is most clearly separated for Li_2CaSiO_4 and least clearly for $LiCaPO_4$. In the latter compound, the tail on the short wavelength side of the emission indicates the presence of another emission overlapping with the dominant Ce^{3+} emission.

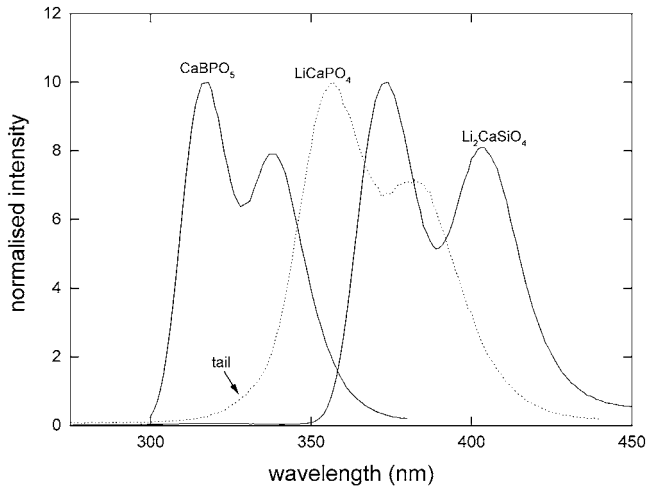

Figure 3. Emission spectra at 12 K of Ce^{3+} in $CaBPO_5$ at $\lambda_{ex} = 280$ nm, in $LiCaPO_4$ at $\lambda_{ex} = 205$ nm and in Li_2CaSiO_4 at $\lambda_{ex} = 205$ nm.

Table 1. Spectroscopic and crystallographic properties of Ce^{3+}-doped compounds. (N:R_{av}) represents the anion coordination number and average distance to the anions (pm). The type of polyhedron (poly) and point symmetry (sym) at the Ce site are given. Wavelengths are in nm and centroid shift ϵ_c, crystal field splitting ϵ_{cfs}, redshift D and Stokes shift ΔS are in cm^{-1}.

Compound	(N:R_{av})	(poly:sym)	λ_5, λ_4, λ_3, λ_2, λ_1	ϵ_c	ϵ_{cfs}	D	ΔS
$CaBPO_5$	(10:261)	(irreg:C_2)	194, 210, 238, 258, 286	8 240	16 600	14 400	3520
$LiCaPO_4$	(8:254)+362	(irreg:C_1)	204, 217, 245, 264, 303	9 870	16 000	16 300	4910
Li_2CaSiO_4	(8:254)	(ddh:D_{2d})	207, 235, 245, 265, 347	11 580	19 500	20 500	2000

Vacuum ultra-violet (VUV) excitation spectra of Ce^{3+} emission are shown in figures 4–6. In the case of $CaBPO_5$ and Li_2CaSiO_4, the five individual 5d bands are clearly observed. Those of Li_2CaSiO_4 are somewhat narrower than those of $CaBPO_5$. The situation with $LiCaPO_4$ is more complicated. Figure 6 shows excitation spectra of the emission at 325, 360 and 410 nm. The excitation spectrum of the 5d $\rightarrow$ $^2F_{5/2}$ emission at 360 nm shows a broad excitation band around 305 nm. The excitation spectra at 325 and 410 nm reveal that this broad emission is actually composed of several subbands. Two peaks at 295 and 303 nm appear in the excitation spectrum of 325 nm emission, and the excitation maximum of 410 nm emission shifts to 325 nm. We will assume that the first excitation band of the main Ce^{3+} centre is located around 303 nm. The locations of the other four 5d bands belonging to this site are indicated by arrows in figure 6. The 295 nm excitation band of 325 nm emission is attributed to another Ce^{3+} centre emitting at shorter wavelengths and responsible for the tail in figure 3. Possibly the emission is related to Ce^{3+} in the $Ca_2P_2O_7$ impurity phase present in the sample.

Information on the wavelengths of the five 5d excitation bands in the three host lattices together with ϵ_c, ϵ_{cfs}, D and ΔS is compiled in table 1. D is obtained with equation (1) and ΔS is obtained from λ_1 and the wavelength of emission to the $^2F_{5/2}$ ground state.

The excitation spectrum of Ce^{3+} emission in $CaBPO_5$:Ce^{3+} shows a band at 145 nm which is attributed to the absorption in the phosphate group. Since this band remains intense in the 'fast' excitation spectrum, energy transfer from the phosphate group to Ce^{3+} is fast and efficient. We conclude that the onset of across bandgap transitions is at 8.25 eV. Pure $LiCaPO_4$

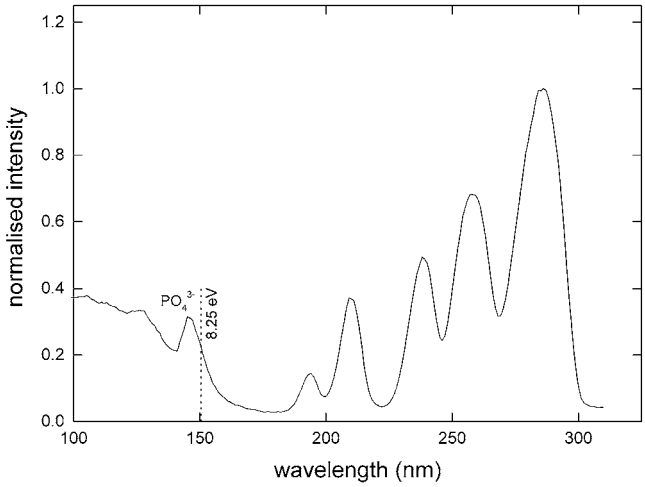

Figure 4. Integral excitation spectrum at 12 K of $CaBPO_5$:Ce^{3+} at $\lambda_{em} = 320$ nm.

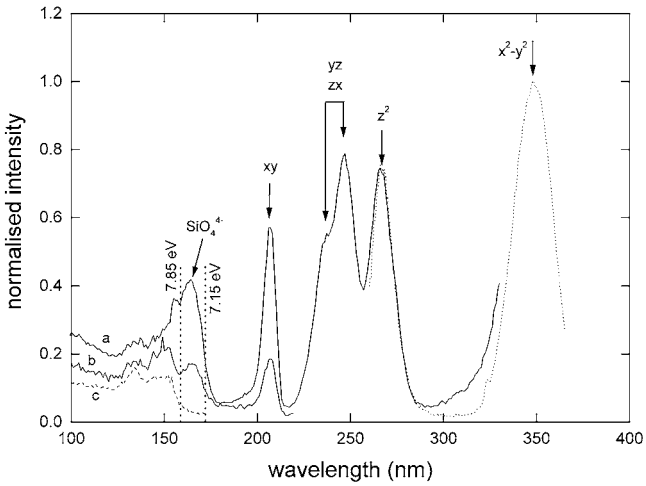

Figure 5. Integral (curve a) and 'slow' (curve b) excitation spectrum of Li_2CaSiO_4:Ce^{3+} at 12 K and $\lambda_{em} = 375$ nm. The spectrum (curve a) from VUV spectroscopy and that from UV/VIS spectroscopy (dashed curve) are normalized to each other at 265 nm. Spectrum c is the 12 K 'slow' excitation spectrum of host emission at 290 nm.

shows at 12 K a 1.16 eV wide excitonic emission at 260 nm. The excitation of this emission is shown as spectrum a in figure 6. A clear threshold is observed at 162 nm. This is as in $CaBPO_5$ attributed to the onset of absorption in the phosphate group. At the same energy one observes a rise in the excitation efficiency of Ce^{3+} emission. The onset corresponds to a bandgap of 7.65 eV.

In Li_2CaSiO_4:Ce^{3+} an excitation band peaking at 165 nm leads to fast Ce^{3+} emission at 375 nm, see curve a in figure 5. The band is attributed to absorption in the SiO_4^{4-} silicate group. As for the phosphate group in $CaBPO_5$ energy transfer to Ce^{3+} is fast and efficient. In the 'slow' excitation spectrum of the same Ce^{3+} emission, a second band appears at 152 nm, see spectrum b in figure 5. Pure Li_2CaSiO_4 shows a slow 1.20 eV wide band emission at

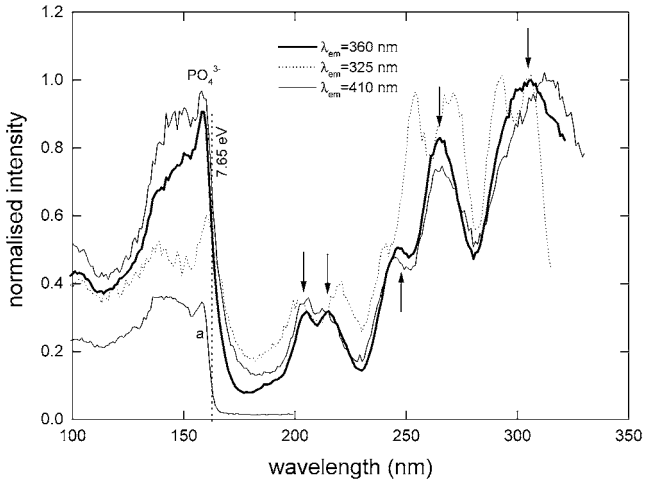

Figure 6. Excitation spectra at 12 K of $LiCaPO_4$:Ce^{3+} at $\lambda_{em} = 325$, 360 and 410 nm. Arrows indicate the locations of 5d excitation bands of the main Ce^{3+} emission. Curve a is the 'slow' excitation spectrum of 260 nm emission in pure $LiCaPO_4$ at 12 K.

290 nm which is attributed to trapped exciton emission of the host crystal. The excitation spectrum of this emission, see spectrum c in figure 5, shows a threshold around 158 nm and reaches a maximum at 152 nm, i.e., at the same wavelength as the second band in spectrum b. We conclude that the onset at 158 nm (7.85 eV) corresponds to the creation of free electrons and free holes. In the pure crystal it will lead to trapped exciton emission. In the Ce^{3+} doped crystal, the free electrons and holes are transferred to Ce^{3+} followed by Ce^{3+} emission with a decay rate determined by the relatively slow transfer. From the onset of the absorption in the silicate group at 174 nm, a bandgap of 7.15 eV is obtained.

Emission decay measurements of Ce^{3+} in $LiCaPO_4$ under direct excitation in any of the five 5d levels at 12 K yield the same single-exponential decay of 25.5 ns. This implies that the relaxation from the higher 5d levels to the lowest emitting 5d level takes place in the subnanosecond time region. Emission decay for $CaBPO_5$:Ce^{3+} is 19.5 ns for excitation in the 5d levels, but also for excitation in the phosphate group at 145 nm. The rapid transfer from the phosphate group to Ce^{3+} suggests that the phosphate group next to a Ce^{3+} centre is excited. The same applies for the silicate group in Li_2CaSiO_4. Excitation of the silicate group and direct excitation in the 5d levels of Ce^{3+} yields a luminescence decay of 27 ns.

5. Discussion

In the analysis of the data to follow we will ignore the influence of a charge compensating defect in the direct neighbourhood of Ce^{3+}. Results available on CaF_2:Ce^{3+} justify this approach. The zero-phonon lines of the first fd transition in CaF_2:Ce^{3+} are located at 309.2, 311.8 and 313.2 nm for, respectively, an uncompensated Ce^{3+}, Ce^{3+} compensated by an interstitial fluorine at the nearest available site and Ce^{3+} compensated by an interstitial fluorine at the next nearest available site [15, 16]. The charge compensator shifts the zero-phonon line by at most 450 cm^{-1}, i.e., much smaller than the typical width of 2000 cm^{-1} of the vibronic side bands dealt with in this work. If Na^+ is used as a charge compensator the shift in the zero-phonon line is less than 100 cm^{-1} [16]. In the case of $CaBPO_5$, Na^+ was added as charge compensating co-dopant. For the other two compounds, a Li^+ vacancy or a Li^+ ion on a Ca^{2+} site are the most likely charge compensating defects.

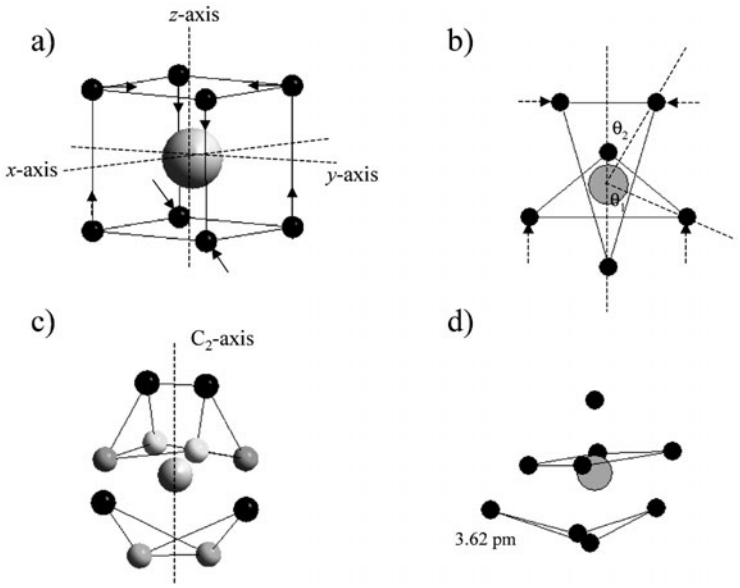

Figure 7. (a) Distortions in a cube leading to a dodecahedron. The oxygen coordination polyhedron around the Ca site in (b) Li_2CaSiO_4, (c) $CaBPO_5$ and (d) $LiCaPO_4$.

The eightfold coordination around the Ca site in Li_2CaSiO_4 is in the form of a dodecahedron. The coordination polyhedron can be described as that of two interpenetrating tetrahedra. In a cube both tetrahedra are equal. In a dodecahedron one tetrahedron is compressed along one of the fourfold symmetry axes of the cube, see figure 7(a). This axis will be defined as the z-axis. The compression leads to a larger value for the angle θ_1 between this axis and the Ce–anion bonds, see figure 7(b). The other tetrahedron is compressed along the face diagonals of the cube leading to smaller angle θ_2. The arrows in figure 7(a) show the direction of both types of compression. The resulting dodecahedron in the case of Li_2CaSiO_4 is shown in figure 7(b). In a cube the xy, yz and zx 5d orbitals of Ce^{3+} are degenerate and form the high energy triplet state. The z^2 and $x^2 - y^2$ orbitals form the low energy degenerate doublet state. The lifting of the degeneracy in a cube when distorting it to a dodecahedron is easy to visualize. The tetrahedron compressed parallel to the z-axis increases the energy of the xy orbital, but the yz and zx orbitals remain close in energy. The tetrahedron compressed along the face diagonals increases the energy of the z^2 orbital relative to that of $x^2 - y^2$. One may now label the 5d excitation bands with the type of 5d orbital as in figure 5.

Dodecahedral coordination is also present in the scheelites $LiYF_4$ and $LiLuF_4$, the xenotime structure of YPO_4 and $LuPO_4$ and the anhydrite $CaSO_4$. Since compounds with this type of coordination tend to show quite similar Ce^{3+} spectroscopy, data from [17] together with those from Li_2CaSiO_4 have been gathered in table 2. In each compound the crystal field splitting falls within the range $19\,000 \pm 1000\ cm^{-1}$. It illustrates that the type of anion (F^- or O^{2-}) and whether oxygen is increasingly more weakly bonded in the sequence sulfate, phosphate and silicate is not of much influence on the crystal field splitting. It has however a large influence on the centroid shift. This increases when fluorine is replaced by oxygen, and it increases with weaker binding of the oxygen ligands in the sequence sulfate, phosphate and silicate. A further characteristic of compounds with dodecahedral coordination with site symmetry close to S_4 is a relatively large energy gap $\Delta E_{1,2}$ between the first ($x^2 - y^2$) and second

Table 2. Spectroscopic and crystallographic properties of scheelites, zirconates and anhydrites with dodecahedral type of coordination. Values for the Stokes shift ΔS are from [11]. All energies are in cm^{-1} and α_{sp} is in 10^{-30} m^3.

Compound	$(\theta_2{:}\theta_1{:}R_2/R_1)$	ΔS	ϵ_{cfs}	$\Delta E_{1,2}$	ϵ_c	α_{sp}
$LiLuF_4$		1240	20 000	7200	5610	0.78
$LiYF_4$	(38°:67°:1.024)	1600	19 500	6700	5520	0.80
$CaSO_4$	(≈28°:≈76°:≈1.06)	800	17 900	5940	8540	1.70
YPO_4	(31°:76°:1.032)	1670	18 000	9040	9570	1.61
$LuPO_4$	(31°:76°:1.039)	1020	19 500	8890	9670	1.85
Li_2CaSiO_4	(30°:67°:1.117)	2000	19 490	8920	11 583	2.12

Table 3. Predicted and observed centroid shift (cm^{-1}) and spectroscopic polarizability (10^{-30} m^3) together with Ce^{3+} decay time (ns) and the bandgap (eV) of the host materials.

Compound	ϵ_c^{pred}	ϵ_c^{obs}	α_{sp}^{pred}	α_{sp}^{obs}	τ	E_g
$CaBPO_5$	8 240	8 240	1.65	1.65	19.5	8.25
$LiCaPO_4$	8 940	9 870	1.92	2.12	25.5	7.65
Li_2CaSiO_4	11 600	11 580	2.63	2.63	27.0	7.15

(z^2) 5d levels. These differences are compiled in table 1. In Li_2CaSiO_4 it is almost one-half of the total crystal field splitting. Figure 1 shows that in relation to the size of the coordination polyhedron, ϵ_{cfs} in Li_2CaSiO_4 appears larger than expectations based on equation (2). This may be related to the relatively large ratio for R_2/R_1 (see table 2). The short Ce^{3+} bond lengths in the tetrahedron compressed parallel to the z-axis probably result in a high energy of the xy orbital.

The coordination around Ca in $CaBPO_5$ is tenfold with C_2 point symmetry, see figure 7(c). The crystal field splitting in this compounds is relatively large for a tenfold coordinated site, cf $LaPO_4$ and LaB_3O_6 have $\epsilon_{cfs} \approx 12\,000$ cm^{-1} [17]. Coordination around the Ca site in $LiCaPO_4$ is very irregular, see figure 7(d). Eight oxygen ions are located within 291 pm with average distance 254 pm and there is an additional one located at 362 pm. Crystal field splitting is of the same order as observed in compounds with cubal coordination, see figure 1. In the sequence Li_2CaSiO_4, $CaBPO_5$ and $LiCaPO_4$ the Stokes shift increases, see table 1. The small Stokes shift of Li_2CaSiO_4 is quite typical for compounds with dodecahedral coordination, see table 2.

α_{sp} has been calculated from the centroid shift and the crystal structure using equation (4). The results shown in figure 2 demonstrate a good agreement with the value calculated from the linear relationship expressed by equation (5). Predicted values for α_{sp} and the centroid shift together with actually observed values are compiled in table 3. The decrease of α_{sp} in the sequence Li_2CaSiO_4, $LiCaPO_4$ and $CaBPO_5$ is caused by the increasingly stronger binding of the oxygen 2p electrons towards the cations other than Ce^{3+}. The stronger binding decreases the covalency between Ce^{3+} and anion ligands; it also decreases anion polarizability and the nephelauxetic effect.

The bandgap of materials is determined by the energy required to remove an electron from the 2p valence band minus the energy gained by placing the electron in the conduction band. Since α_{sp} is a measure for the binding strength of the 2p oxygen electrons, the first energy will tend to decrease with increasing value for α_{sp}. For the three compounds studied in this work, the bandgap indeed decreases with increase of α_{sp}, see table 3.

The decay time of the Ce^{3+} d $\rightarrow$ f emission increases by a factor of 1.4 in the sequence $CaBPO_5$, $LiCaPO_4$ and Li_2CaSiO_4, see table 3. Theoretically it is proportional with λ_{em}^3 and a

factor of 1.6 is to be expected. On the other hand decay time is also inversely proportional to $n(n^2+2)^2$ where n is the refractive index of the compound [18]. Since polarizability α_{sp} and n are closely related parameters, n is expected to increase slightly in the sequence $CaBPO_5$, $LiCaPO_4$ and Li_2CaSiO_4. This will partially cancel the effects of the changing emission wavelength. Finally, the matrix element connecting the 5d state with the 4f state via the dipole operator is important [18, 19]. The values for this matrix element are not known, but since the change in τ is already reasonably accounted for by λ_{em}^3 and $n(n^2+2)^2$ apparently the matrix element must have quite a similar value in the three compounds.

Summarizing, the energies of all five 5d levels of Ce^{3+} in $CaBPO_5$, $LiCaPO_4$ and Li_2CaSiO_4 have been identified together with the bandgap of the host crystals. The bandgap is determined by the absorption in the phosphate and silicate groups. From the centroid shift of the 5d configuration the spectroscopic polarizability α_{sp} was determined and it shows very good agreement with values calculated from the electronegativity of the cations in the compound. The crystal field splitting in all three compounds is comparable with the crystal field splitting usually observed for eightfold cubal or eightfold dodecahedral coordination.

Acknowledgments

These investigations were supported by a van Gogh subsidy from the Netherlands Organization for Scientific Research (NWO) and by IHP contract HPRI-CT-1990-00040 of the European Commission.

References

[1] van Loef E V D, Dorenbos P, van Eijk C W E, Krämer K and Güdel H U 2000 *Appl. Phys. Lett.* **77** 1467
[2] van Loef E V D, Dorenbos P, van Eijk C W E, Krämer K and Güdel H U 2001 *Appl. Phys. Lett.* **79** 1573
[3] Pauwels D, Le Masson N, Viana B, Kahn-Harari A, van Loef E V D, Dorenbos P and van Eijk C W E 2000 *IEEE Trans. Nucl. Sci.* **47** 1787
[4] Efryushina N P, Maskalyuk L G, Berezovskaya I V and Dotsenko V P 1998 *Ukr. Chem. J.* **64** 10
[5] Tyner C E and Drickamer H G 1977 *J. Chem. Phys.* **67** 4116
[6] Blasse G, Bril A and de Vries J 1969 *J. Inorg. Nucl. Chem.* **31** 568
[7] Su Qiang, Liang Hongbin, Hu Tiandou, Tao Ye and Lin Tao 2002 *J. Alloys Compounds* **344** 132
[8] Waite M S 1974 *J. Electrochem. Soc. Solid State Sci. Technol.* **121** 1122
[9] Lang R J 1936 *Can. J. Res.* **14** 127
[10] Dorenbos P 2000 *Phys. Rev.* B **62** 15640
[11] Dorenbos P 2000 *J. Lumin.* **91** 155
[12] Dorenbos P 2000 *Phys. Rev.* B **62** 15650
[13] Dorenbos P 2002 *J. Lumin.* **99** 283
[14] Dorenbos P 2002 *Phys. Rev.* B **65** 235110
[15] Manthey W J 1973 *Phys. Rev.* B **8** 4086
[16] Pack D W, Manthey W J and McClure D S 1989 *Phys. Rev.* B **40** 9930
[17] Dorenbos P 2001 *Phys. Rev.* B **64** 125117
[18] See e.g. equation (4.74)
Henderson B and Imbush G F 1989 *Optical Spectroscopy of Inorganic Solids* (Oxford: Clarendon)
[19] Williams G M, Edelstein N, Boatner L A and Abraham M M 1989 *Phys. Rev.* B **40** 4143